HHS Public Access

Author manuscript

Environ Sci Technol. Author manuscript; available in PMC 2022 March 11.

Published in final edited form as:

Environ Sci Technol. 2019 February 19; 53(4): 2220–2228. doi:10.1021/acs.est.8b05355.

Characterizing flaring from unconventional oil and gas operations in south Texas using satellite observations

Meredith Franklin[*,§], **Khang Chau**[§], **Lara J. Cushing**[¶], **Jill E. Johnston**[§]

[§]Department of Preventive Medicine, University of Southern California, Los Angeles California 90032, United States

[¶]Department of Health Education, San Francisco State University, San Francisco California, 94132, United States

Abstract

Over the past decade, increases in high-volume hydraulic fracturing for oil and gas extraction in the United States have raised concerns with residents living near wells. Flaring, or the combustion of petroleum products into the open atmosphere, is a common practice associated with oil and gas exploration and production, and has been under-examined as a potential source of exposure. We leveraged data from the Visible Infrared Imaging Spectroradiometer (VIIRS) Nightfire satellite product to characterize the extent of flaring in the Eagle Ford Shale region of south Texas, one of the most productive in the nation. Spatiotemporal hierarchical clustering identified flaring sources, and a regression-based approach combining VIIRS information with reported estimates of vented and flared gas from the Railroad Commission of Texas enabled estimation of flared gas volume at each flare. We identified 43,887 distinct oil and gas flares in the study region from 2012–2016, with a peak in activity in 2014 and an estimated 4.5 billion cubic meters of total gas volume flared over the study period. A comparison with well permit data indicated the majority of flares were associated with oil-producing (82%) and horizontally-drilled (92%) wells. Of the 49 counties in the region, 5 accounted for 71% of the total flaring. Our results suggest flaring may be a significant environmental exposure in parts of this region.

Introduction

With the rise in unconventional oil and gas (UOG) extraction techniques, domestic oil and gas production has increased in the United States (U.S.) to its highest level in over a decade.[1] Unconventional extraction techniques include horizontal or directional drilling and high-volume hydraulic fracturing, a well stimulation technique whereby pressurized fluids are injected into wells to fracture rock and allow for enhanced oil and gas recovery.

[*]Corresponding author: Phone: +1 (323) 442-2703; meredith.franklin@usc.edu.

ASSOCIATED CONTENT

Supporting Information includes Table S1: Listing of counties in the Eagle Ford Shale with number of flares 2012–2016; Figure S1 Map of clustered flares, noise points, and cluster centers in LaSalle, County TX in 2014; Figure S2: histogram of distances between VIIRS clustered and noise flares and the nearest permitted well; Table S2: Summary statistics of distances between VIIRS flares and permitted wells; Table S3: Parameter estimates and summary statistics of best performing regression models used to estimate flared gas volume (BCM) from VIIRS temperature and source area. The following pdf contains all of supporting information and is available free of charge.

These techniques have enabled the exploration and extraction of oil and gas from areas that were previously inaccessible or uneconomic, including low permeability geological formations composed of shale, sandstone, and carbonate. Unlike conventional drilling, UOG production occurs at smaller scales, resulting in thousands of extraction sites in relatively small geographic areas.[2] Subsequently, oil and gas extraction has become more common near where people live and work, increasing the potential for human exposure to contaminants including air pollution, water pollution, and noise associated with UOG production.[3] A recent study estimated that 17.6 million people live within approximately 1.6 km of an active oil and/or gas well in the continental U.S.[4] There is preliminary but growing evidence of increased health risks associated with living in close proximity to UOG infrastructure including cancer risk[5] and higher rates of chronic respiratory illness,[6] migraines and fatigue,[6] and adverse birth outcomes.[7–9]

Flaring is a widely used practice for the disposal of natural gas during drilling and production in places where there is insufficient infrastructure for the capture and transport of the gas, yet studies on the health impacts of flaring are limited. Global estimates indicate that more than 139 billion m^3 (BCM) of gas are flared annually, or about 4.6% of the world's natural gas consumption.[10] The U.S. has the largest number of individual flare locations globally, burning an estimated 6.5 BCM of natural gas in 2012.[11] Flaring is highly visible to local residents and may represent an important health concern because flares can release harmful air pollutants including volatile organic compounds, polycyclic aromatic hydrocarbons, carbon monoxide, nitrous oxides, sulfur oxides, toxic heavy metals, formaldehyde and black carbon soot[12–15] and typically last for multiple days or years.[16] Recent studies have attributed worsened air quality to the abundance of flaring from UOG operations.[3,17,18]

A major barrier to assessing the health risks of flaring is the lack of comprehensive data collection on flaring activities in the U.S. Remote sensing provides a unique, objective, and alternate means of characterizing flaring. Multi-spectral satellite instruments with infrared bands collecting data at night are able to detect sources of abnormally high temperatures (i.e. thermal anomalies) from space.[10,19] Due to challenges in identifying small heat sources relative to the spatial resolution of satellite instruments, in addition to challenges in separating brightness from other sources (background, artificial lights, fires), early approaches to flaring detection required visual inspection of satellite images. Recent algorithmic advances have resulted in two global products that provide data on heat sources related to flaring. The operational Moderate Resolution Imaging Spectroradiometer (MODIS) fire detection product provides identification of 1 km gridded "fire pixels" including estimates of fire radiative power.[20,21] A sub-pixel-based calculation of the MODIS fire radiative power has been developed [22] and applied to detect wildfire events in California.[23] The Visible Infrared Imaging Radiometer Suite (VIIRS) onboard the Suomi National Polar Partnership satellite (SNPP) is a multi-spectral instrument with bands for day and night observation collected at 750 m spatial resolution. The Nightfire algorithm, developed by the National Oceanic and Atmospheric Administration (NOAA) Earth Observation Group, [24] uses the near-infrared and shortwave infrared bands to detect locations of sub-pixel (<750 m) combustion sources.[25] The VIIRS Nightfire data have been used to improve global estimates of flared gas volume [11] and detect industrial heat

sources.[26] In a comparison of MODIS and VIIRS products, Sharma et al.[12] found through validation by visual inspection using Google Earth that VIIRS Nightfire had better accuracy and efficacy in identifying and characterizing gas flares in a large oil and gas producing region of Russia.

In this study we focus on the Eagle Ford Shale play, a roughly 52,000 km^2 area encompassing dozens of predominantly rural counties in southern and central Texas. The Eagle Ford Shale is one of the most active and productive shale plays in the U.S., ranking highest for the volume of oil produced and fourth highest for gas production as of 2013.[27] Roughly 1.2 million barrels of oil and 6,000 million ft^3 (0.17 BCM) of gas were extracted daily from this region at its peak in 2015; a more than 75- and 15- fold increase, respectively, since 2010.[28,29] We used VIIRS Nightfire, applying spatiotemporal hierarchical clustering to pinpoint sources of flaring and exclude isolated observations. We assessed the proximity between flaring sources and permitted well sites, and characterized spatial and temporal trends in flaring activity during the study period. Finally, we used VIIRS flare properties to estimate the volume of gas at each flaring site through a regression-based approach that linked field-level estimates of total vented and flared gas that are self-reported to the Railroad Commission of Texas (TXRRC).

Materials and Methods

Study Region

The Eagle Ford Shale play extends through southern and central Texas. We examined 49 primarily rural counties: 22 identified by the TXRRC as part of the Eagle Ford Shale and 27 adjacent counties with an active oil or gas permit during the study period, April 1, 2012 through December 31, 2016. A list of the counties included in the study is given in Supporting Information Table S1.

Satellite Data

The VIIRS instrument is onboard the Suomi National Polar Partnership satellite (SNPP), which was launched in late 2011. It has 22 spectral bands collecting data from the visible to long-wave infrared (0.412 μm to 12.01 μm) with 750 m spatial resolution at nadir. Nine of the spectral bands collect data at night, with a signature at 1.6 μm (the VIIRS M10 band) that is uniquely capable of detecting combustion related heat sources.[25] When a thermal source is identified in the M10 band, and confirmed by a detection in at least one of five additional bands (visible or day-night-band DNB, M7 and M8 in the near infrared, and M12 and M13 in the mid-wave infrared), Plank curve fitting is applied to estimate source temperature (T, degrees K).[11] If only detected in the M10 band but not in another spectral band, Plank curve fitting is not possible, so temperatures are assigned from the average temperature for multi-band observations at the same site or by the nearest detection having Plank curve fits.[11] In addition to temperature, the Nightfire product provides source area (S, m^2), estimated from an emission scaling factor based on spectral emissivity and size of the pixel footprint, and radiant heat intensity (RH, W/m^2), estimated using Stephan-Boltzmann's Law $RH=\sigma T^4 S$.

For this study, the “flares only” V2.1 Nightfire product was used, providing nightly data from March 2012 onward. As Nightfire detects thermal sources on a sub-pixel spatial scale, they are not on a fixed grid like many satellite products and are thus more representative of a spatially varying point source than a fixed source. Previous examinations of the Nightfire product indicated a bimodal temperature distribution with volcanoes and biomass burning in the range from 600 K to 1500 K, and gas flares in the range from 1500 K to 2000 K.[11,25] Given difficulty in distinguishing between high temperature biomass burning and gas flaring in the crossover zone between 1300 and 1500 K, we only examined detections 1600 K and hotter, which has been shown to be an effective way to ensure gas flares are identified.[11]

Oil and Gas Well Permit Data

Oil and gas well lease information in the Eagle Ford region was obtained from DrillingInfo.[30] We extracted data on drill type (horizontal, vertical, directional, unknown), well status (active, inactive, abandoned), plug date (date production permanently ends), completion date or first production date (when well is ready or begins production), last production date as well as latitude and longitude. Our analysis included any permitted well locations that had an active lease between 1990 to 2016. We excluded inactive wells with a plug date or last reported production date before the beginning of our study period, April 1, 2012.

State Oil and Gas Production Data

The TXRRC regulates the oil and gas industry in the state of Texas and requires oil and gas producers to report an estimate of the volume of vented or flared gas on a monthly basis.[31] Reporting occurs at the field level, with hundreds of wells associated with any one field. Therefore, to use the TXRCC reported volumes in the development of a method to estimate flared gas volume from VIIRS Nightfire information, we linked fields to their county and summed Nightfire data over the month and county. Approximately 2% of the fields were associated with two counties. For each of these fields, we assigned a probability of which county it belonged to based on the number of county-level VIIRS-identified flares for the given month of reporting. Reports of monthly emissions from fields that straddled two counties were distributed proportionally to each county based on the number of VIIRS identified flares in that county during the same month.

Statistical Methods: Clustering

With the prominence of complex geospatial datasets in earth sciences such as remote sensing imagery, density-based clustering algorithms have become increasingly popular to extract and interpret useful information.[32] Due to the sub-pixel nature of the VIIRS Nightfire data, application of clustering methods was necessary to differentiate flares attributable to an aggregate flaring source from aberrant observations. Flaring sources from oil and gas drilling tend to have persistent activity over space and time, whereas non-oil and gas sources such as high temperature biomass burning occur sporadically. As such, density-based clustering methods are attractive as they are capable of classifying observations into irregularly shaped clusters while simultaneously refusing to cluster some observations, identifying unclustered points as noise.[33] Furthermore, they do not require any distributional assumptions. In many applications this methodology has clear advantages

over traditional k-Means type clustering, which requires that the clusters have a Gaussian distribution, that all points are assigned to a cluster, and that the number of clusters be determined before applying the algorithm. Density-based clustering methods are non-parametric, with data arising from an unknown probability density function defined over the metric space, and clusters defined as the connected components of high density regions. The measure-theoretic statistical basis of density-based clustering is presented in Rinaldo and Wasserman.[34] One important enhancement of density based clustering is the single linkage method, whereby a hierarchical structure is added to high-density clusters, creating a cluster tree.[35] A generalized form of the single linkage method followed,[36] as well as a robust variant[37] of hierarchical clustering. Computational implementation of density-based clustering includes Density Based Spatial Clustering of Applications with Noise (DBSCAN), which was pioneered in the late 1990s as a class identification method for spatial data.[32] The single-linkage method has been implemented in a hierarchical version of DBSCAN called HDBSCAN*.[38,39]

We applied HDBSCAN* with robust single-linkage to conduct annual cluster detection of the VIIRS Nightfire data. Given a set of georeferenced (latitude, longitude) points $\mathbf{X}$, HDBSCAN* only requires a single parameter input k, the minimum number of points in a cluster. For each point x_p in $\mathbf{X}$, the HDBSCAN* algorithm first calculates the core distance $d_{\text{core}}(\mathbf{x}_p)$, which is the distance from x_p to its k^{th}-nearest neighbor. The algorithm next computes an extended version of a minimum spanning tree (MST)[40] via connecting each point to its nearest neighbor in the single-linkage manner generating a single "root" cluster ($\boldsymbol{C}_1$) that contains all points in $\mathbf{X}$, and all of the $\mathbf{x}_p$ are considered "core" points. Denoting ϵ as the radius around each point $\mathbf{x}_p$, the algorithm proceeds to break up the root cluster and subsequent clusters $\boldsymbol{C}_2,\ldots,\boldsymbol{C}_n$ by scanning all observed values of ϵ in a decreasing manner and removing the connection between points when their inter-point distance is greater than ϵ (tied connections are removed simultaneously). When breaking a connection at a particular ϵ there are two possible outcomes: (1) if it results in two clusters each with at least as many points as k, the points in each cluster are assigned a new cluster label; (2) if it only removes one point from an existing cluster, the point is now considered an unclustered point at ϵ. The resulting dendrogram represents the hierarchy by connecting all points in $\mathbf{X}$ and indicating the distance ϵ at which smaller clusters appear or points are not clustered.[37]

With this hierarchy, HDBSCAN* presents a "flat" solution where the most prominent clusters are extracted and the unclustered points are labeled as noise. The unsupervised cluster extraction process consists of two steps: (1) calculating the stability $\boldsymbol{S}(\boldsymbol{C}_i)$ of each cluster $\boldsymbol{C}_i$ (except $\boldsymbol{C}_1$) by adapting the notion of excess of mass; [36] (2) iteratively and recursively comparing the stability of the smaller clusters and larger clusters (by adding points as ϵ increases and combing clusters) and choosing the most stable non-overlapping clusters. This process improved upon DBSCAN by making local cuts that are sensitive to the density of each clusters instead of a local cut across the cluster tree at a predefined ϵ. Furthermore, hierarchical density based clustering has been shown to perform better both computationally and with data having varying density than non-hierarchical methods.[33] We applied HDBSCAN* to annually stratified data, tuning the algorithm for k between 2 and 10 and choosing a value for each calendar year that minimized the number of noise points.

Finally, the identified clusters were validated with DrillingInfo permit data by examining the distance between the clustered flares and the nearest permitted well that was active during our study period.

Statistical Methods: Estimation of Flared Gas Volume

To estimate flared gas volume from VIIRS Nightfire data, Elvidge et al[11] developed a calibration method of radiant heat that included a modification of source area based on solar zenith angle and elliptical geometry. As this method required data not in the publicly available Nightfire product in addition to complex geometric calculations, we instead developed a regression approach using VIIRS Nightfire parameters. The intent of this approach is to closely approximate the Elvidge et al[11] procedure and provide an equation that can be used to convert available source area and temperature to flared gas volume in billion cubic meters (BCM).

In model development we included clustered VIIRS flares linked with county-level flared gas volume reported by the TXRRC. We summed the VIIRS parameters by month for each county in the study region. With these matched data, we explored several regression model approaches, including linear, polynomial, and semi-parametric regression with generalized additive models (GAM) to estimate BCM from VIIRS source temperature, source area and/or radiant heat. Different model approaches were compared by their overall R^2 values, and 10-fold cross-validation was applied to the final model with cross-validation R^2 as the metric of performance. We repeated the 10-fold cross-validation 1,000 times assessing the mean, median, and range of the observed versus predicted R^2.

Results

Oil and Gas Drilling Trends

Based on DrillingInfo well permit data, from 1990 to 2016 there were a total of 19,217 permitted oil wells (46%), 14,969 permitted gas wells (36%), and 7,271 permitted combined oil and gas wells (18%) in the Eagle Ford Shale that were active during the 2012–2016 study period (Figure 1). By drill direction, 2,667 wells were directional (6%), 20,658 horizontal (50%) and 18,132 vertical (44%).

The region saw a sharp increase in horizontal drilling of oil wells beginning in 2010 and peaking in 2014. While these well types have decreased since 2014, they remain more prominent in the region than gas and vertical drilling. Cross tabulation of permitted wells by type and direction are shown in Table 1. Horizontal oil wells comprise the largest proportion of the wells, and tend to be located along the central to northern part of Eagle Ford Shale (Figure 1 (a) and (b)).

VIIRS Flare Identification

There were 46,754 distinct flares with temperatures > 1600 K identified by the VIIRS Nightfire algorithm in the study region from 2012 through 2016 (Figure 2). Application of HDBSCAN* separated these flares into annual clusters, which we considered to represent persistent sources, and noise points, which we considered to be aberrant flaring occurrences.

An illustration of the VIIRS flares with cluster and noise points can be seen in Supporting Information Figure S1.

The tuned minimum number of points, *k,* for annual runs of HDBSCAN* that minimized the number of noise points ranged from 3 to 6 (Table 2). Over the study period, the proportion of noise points remained relatively steady from 4.1–6.9%, as did the number of clusters, ranging from 393 to 419. Noise observations (N = 2,810) were excluded from the remainder of our analysis, leaving a total of 43,944 flares.

VIIRS Nightfire identified flares (Figure 3) follow the spatial pattern of horizontal oil permits seen in Figure 2. The most prominent flaring "hotspots" are in western and central portions of the Eagle Ford Shale, namely LaSalle, McMullen, and Karnes counties.

Characterization of Flaring by Well Type

We linked the flares to permitted wells in the DrilingInfo database to validate our approach by confirming that flaring locations detected by VIIRS were in close proximity to known UOG sites. There were 70% of flares within 500 m and 87% within 750 m of a permitted well location. A small number of flares were farther than 2.5 km from a permitted well location (0.5% of clustered flares and 1.5% of noise flares). Excluding noise points through the application of HDBSCAN* reduced the median distance (and variability) between flares and the nearest well from 366m (IQR = 337 m) to 356 m (IQR = 324 m). These distances suggest a reasonable degree of spatial precision given the original resolution of the VIIRS instrument (750 m at nadir), and an improvement in precision with the application of HDBSCAN* (Supporting Information Figure S2 and Table S2).

The vast majority of the wells nearest to flares produced oil (82%) or were horizontally drilled (92%), indicating that flaring in Eagle Ford is predominantly from oil production as hypothesized (Table 3).

Flared Gas Volume

Flared gas volume was best estimated from regressions that included VIIRS temperature and source area. Parameter estimates and model R^2 comparing linear, polynomial, and GAM models are summarized in Supporting Information Table S2. While GAM had the best performance ($R^2 = 0.809$), polynomial regression with a cubic function of temperature and linear function of source area performed nearly as well ($R^2 = 0.803$) and has interpretable coefficients that allow for transferability of the regression model to studies using VIIRS Nightfire data in other geographic regions. The model using all data is as follows:

$$\textit{Monthly Flare Vol (BCM)} = 3.63\times10^{-4} + 6.02\times10^{-8}\,T + 8.67\times10^{-14}\,T^2 - 1.18\times10^{-19}\,T^3 - 1.63\times10^{-5}\,S$$

where T (temperature, degrees K) and S (area, m^2) are both monthly sums of all flares within a county. Monthly predicted flare volumes based on this model were further summed by year over the whole Eagle Ford Shale and are presented in Table 4. In 1000 repetitions of 10-fold cross validation, the mean observed versus predicted cross-validation R^2 was 0.892. While we predict county-level BCM, this equation can be applied to predict monthly flared gas volumes at different (finer) spatial scales, similar to Elvidge et al.[11]

Following the pattern seen in Table 2, flared gas volume increased as the number of distinct flares increased from 0.81 BCM in 2012 to a peak of 1.19 BCM in 2014, and then decreased to 0.52 BCM by 2016 (Table 4). These estimates are significantly higher than a previous analysis of TXRRC data from 2009–2012 by the San Antonio Express-News,[41] and consistent with the increase in UOG activity in the study region that started in 2010.

Temporal and Spatial Trends in Flaring

We observed a significant rise in flaring activity from 2012 (N=7,773) to a peak in 2014 (N=11,816), followed by a sharp decrease in 2016 (N=5,030) (Table 4). This trend followed what was observed in the DrillingInfo permit data (Figure 1). Average temperature (K), radiant heat intensity (W/m^2), source area (m^2), and estimated gas volume (BCM) of individual flares increased from 2012 to 2016 (Table 4). This suggests a transition in the proportion of flares arising from exploration activities (a higher number of lower intensity flares) as opposed to production (a smaller number of higher intensity flares) between 2012–2014 versus 2015–2016. This decrease in exploration is consistent with the reported number of drill rigs in the Eagle Ford Shale – and indicator of exploration activity – as reported by the Energy Information Agency and coincided with a significant drop in oil prices in 2015.[42]

Flaring impacted many counties in Eagle Ford either by number of flares or the number of nights where there was some flaring activity identified (Figure 4). Spatial analysis showed that 45 of the 49 counties in the region had some flaring during the study period. The most highly impacted counties were consistently (from west to east) Dimmit, La Salle, McMullen, Karnes, and Dewitt, which combined accounted for 71% of all flares (12%, 25%, 19%, 15%, and 7%, respectively). By way of comparison, an estimated 1.11 BCM of flared gas was emitted in La Salle County alone from 2012 to 2016, nearly the same amount emitted over the whole region in the peak of 2014 (Supporting Information Table S1).

The number of nights where flaring occurred was also highest in La Salle, McMullen, and Karnes counties, with 1276, 1226 and 1214 nights of flaring activity in each of these counties, respectively. This represents 66–70% of the nights over the five-year study period. Flaring occurred for at least 30 nights in a one-year period in 27 of the 49 counties.

Limitations

A few limitations in the data and methods are worth noting. A common phenomenon in wide-scanning satellite instruments is the “bow tie” effect, where detections far from nadir along the outer portion of the swath may be double counted. While top most and bottom most pixel duplicates are automatically excluded by the onboard VIIRS software, there remains some overlap near the edge of the scan. Through manual processing, Polivka et al [43] found approximately 11% of the VIIRS detections in the M-bands suffered from duplication. If our study area includes scan overlap, there may be a modest overestimation in the number of flares detected since the Nightfire algorithm does not include additional “bow tie” effect pixel removal. Another phenomenon occurring at swath edges is the saturation artifact, where pixels at the scan edge are two to four times the size of nadir pixels. For VIIRS, saturation has been shown to be most problematic in the M12 band and not experienced in the M10 band, which is the primary band for the Nightfire algorithm.[44] Saturation artifacts

are therefore presumed to result in negligible overrepresentation of flare detections in this study.

The oil and gas industry is not the only source of thermal anomalies – VIIRS Nightfire can detect industrial activities such as steel and cement manufacturing, smelters, or chemical processing plants.[26] However, our study area includes very little of these types of industrial activity. Moreover, prior research suggests 99% of thermal anomalies from oil and gas have temperatures >1250 K, whereas other industries such as steel and cement manufacturing have thermal signatures at much lower temperatures.[26] To assess the potential for misclassification of non-UOG sources in our dataset, we compared the locations of VIIRS identified flares (>1600 K) to the locations of industrial facilities in the Environmental Protection Agency Toxic Release Inventory (TRI). Only 0.6% of the flares were located within 1 km of 13 potential industrial thermal sources.

While the aforementioned limitations may have led to an overestimate of flares in our study, we believe they were likely balanced by processing steps that could have led to underestimation of the quantity of flaring. In a study of VIIRS Nightfire and Sentinel-3 observations over other areas with on- and off-shore drilling, Caseiro et al[45] found that some oil and gas related flares have signals in the 1000 – 1200 K range. We removed VIIRS Nightfire detections < 1600 K to exclude potential biomass burning and industrial heat sources based on previous studies.[11,25] Furthermore, in clustering with HDBSCAN*, we removed 4–7% VIIRS detections that were identified as noise. It is possible that we removed valid flares, leading to an analytic dataset that underestimates the quantity of flaring in the region. Finally, in our estimation of BCM, we note that the TXRRC does not disaggregate vented from flared gas, which could result in an overestimation of flared gas volume. However, the data are self-reported, which likely results in an underestimate of the true volume of gas flared.

Implications for Research and Policy

With the rise in UOG extraction techniques, overall domestic oil and gas production has increased to its highest level in over a decade, with another major upswing in UOG activity in the U.S. projected by 2050 associated with continued technological advances and higher oil prices.[1] Without major investment in infrastructure, flaring is likely to continue as a primary mechanism of waste gas disposal in the Eagle Ford Shale and other regions of heavy flaring, such as the Bakken formation in North Dakota. Estimates of flared gas volumes are even larger in Russia, Iraq, Iran, Nigeria and Venezuela than in the U.S.[11] The flaring of gas is likely to impact local air quality and contribute substantial greenhouse gas emissions. For example, an estimated 267 million total metric tons of CO_2 were flared worldwide in 2008.[46] Lifecycle analyses also estimate a larger greenhouse gas footprint for natural gas extracted from shale formations than for coal,[47] although these estimates generally have not incorporated emissions from flaring. Thorough understanding of the climate, air quality, and health impacts of flaring has been limited by the fact that oil and gas facilities in the U.S. are self-auditing and provide minimal information on waste disposal processes to governmental agencies. A lack of air quality monitoring in rural areas of intense UOG activity also hinders investigations into the impacts of UOG activities.[48]

Our spatiotemporal modeling approach utilizing VIIRS satellite observations – which has global coverage – illustrates how remote sensing data can objectively characterize flaring activity and address the current paucity of systematic reporting of flaring locations, timing and volumes. Combining these new satellite tools with air monitoring and health data would allow for a better characterization of the impacts of flaring to local air quality, the climate, and human health and welfare. Applications of this approach can inform regulatory efforts to track and control flaring activity, inventory and reduce greenhouse gas emissions, and conduct air quality monitoring to better understand exposures and reduce potential human health impacts.

Supplementary Material

Refer to Web version on PubMed Central for supplementary material.

ACKNOWLEDGEMENT

The authors would like to thank Dr. Mikhail Zhizhin of the National Oceanic and Atmospheric Administration (NOAA), National Environmental Satellite, Data, and Information Service (NESDIS), National Centers for Environmental Information (NCEI) for his support and insights on using the VIIRS Nightfire data.

Funding source

This research was supported by NIH/NIEHS R21ES028417.

REFERENCES

(1). EIA. Oil and Natural Gas Resources and Technology: Issue in Focus from the Annual Energy Outlook 2018. U.S Energy Information Administration; 2018.

(2). Jones NF; Pejchar L; Kiesecker JM The Energy Footprint: How Oil, Natural Gas, and Wind Energy Affect Land for Biodiversity and the Flow of Ecosystem Services. Bioscience 2015, 65 (3), 290–301.

(3). Moore CW; Zielinska B; Pétron G; Jackson RB Air Impacts of Increased Natural Gas Acquisition, Processing, and Use: A Critical Review. Environ. Sci. Technol. 2014, 48 (15), 8349–8359. [PubMed: 24588259]

(4). Czolowski ED; Santoro RL; Srebotnjak T; Shonkoff SBC Toward Consistent Methodology to Quantify Populations in Proximity to Oil and Gas Development: A National Spatial Analysis and Review. Environ. Health Perspect. 2017, 125 (8), 1–11. [PubMed: 27384039]

(5). McKenzie LM; Witter RZ; Newman LS; Adgate JL Human Health Risk Assessment of Air Emissions from Development of Unconventional Natural Gas Resources. Sci. Total Environ. 2012, 424, 79–87. [PubMed: 22444058]

(6). Tustin AW; Hirsch AG; Rasmussen SG; Casey JA; Bandeen-roche K Associations between Unconventional Natural Gas Development and Nasal and Sinus, Migraine Headache, and Fatigue Symptoms in Pennsylvania. Environ. Health Perspect. 2017, 125 (2), 189–197. [PubMed: 27561132]

(7). Whitworth KW; Marshall AK; Symanski E Drilling and Production Activity Related to Unconventional Gas Development and Severity of Preterm Birth. Environ. Health Perspect. 2018, 126 (3), 1–8.

(8). Stacy SL; Brink LL; Larkin JC; Sadovsky Y; Goldstein BD; Pitt BR; Talbott EO Perinatal Outcomes and Unconventional Natural Gas Operations in Southwest Pennsylvania. PLoS One 2015, 10 (6), e0126425. [PubMed: 26039051]

(9). Casey JA; Savitz DA; Rasmussen SG; Ogburn EL; Pollak J; Mercer DG; Schwartz BS Unconventional Natural Gas Development and Birth Outcomes in Pennsylvania, USA. Epidemiology 2016, 27 (2), 163–172. [PubMed: 26426945]

(10). Elvidge CD; Ziskin D; Baugh KE; Tuttle BT; Ghosh T; Pack DW; Erwin EH; Zhizhin M A Fifteen Year Record of Global Natural Gas Flaring Derived from Satellite Data. Energies 2009, 2 (3), 595–622.

(11). Elvidge CD; Zhizhin M; Baugh K; Hsu FC; Ghosh T Methods for Global Survey of Natural Gas Flaring from Visible Infrared Imaging Radiometer Suite Data. Energies 2016, 9 (14), 1–15.

(12). Strosher M Investigations of Flare Gas Emissions in Alberta. Final Report. 1996, pp 1–158.

(13). Ite E, A.; Ibok J, U. Gas Flaring and Venting Associated with Petroleum Exploration and Production in the Nigeria's Niger Delta. Am. J. Environ. Prot. 2013, 1 (4), 70–77.

(14). Strosher MT Characterization of Emissions from Diffusion Flare Systems. J. Air Waste Manag. Assoc. 2000, 50 (10), 1723–1733.

(15). Kindzierski WB Importance of Human Environmental Exposure to Hazardous Air Pollutants from Gas Flares. Environ. Rev. 1999, 8 (1), 41–62.

(16). Johnson MR; Coderre AR An Analysis of Flaring and Venting Activity in the Alberta Upstream Oil and Gas Industry. J. Air Waste Manage. Assoc. 2011, 61 (2), 190–200.

(17). Hildenbrand ZL; Mach PM; McBride EM; Dorreyatim MN; Taylor JT; Carlton DD; Meik JM; Fontenot BE; Wright KC; Schug KA; et al. Point Source Attribution of Ambient Contamination Events near Unconventional Oil and Gas Development. Sci. Total Environ. 2016, 573 (15), 382–388. [PubMed: 27572531]

(18). Schade GW; Roest G Analysis of Non-Methane Hydrocarbon Data from a Monitoring Station Affected by Oil and Gas Development in the Eagle Ford Shale, Texas. Elem. Sci. Anthr. 2016, 4 (1), 000096.

(19). Casadio S; Arino O; Serpe D Gas Flaring Monitoring from Space Using the ATSR Instrument Series. Remote Sens. Environ. 2012, 116, 239–249.

(20). Giglio L; Schroeder W; Justice CO The Collection 6 MODIS Active Fire Detection Algorithm and Fire Products. Remote Sens. Environ. 2016, 178, 31–41. [PubMed: 30158718]

(21). Sharma A; Wang J; Lennartson EM Intercomparison of MODIS and VIIRS Fire Products in Khanty-Mansiysk Russia: Implications for Characterizing Gas Flaring from Space. Atmosphere (Basel). 2017, 8 (95), 1–19.

(22). Peterson D; Wang J; Ichoku C; Hyer E; Ambrosia V A Sub-Pixel-Based Calculation of Fire Radiative Power from MODIS Observations: 1. Algorithm Development and Initial Assessment. Remote Sens. Environ. 2013, 129, 262–279.

(23). Peterson D; Wang J A Sub-Pixel-Based Calculation of Fire Radiative Power from MODIS Observations: 2. Sensitivity Analysis and Potential Fire Weather Application. Remote Sens. Environ. 2013, 129, 231–249.

(24). NOAA. National Oceanic and Atmospheric Administration: Earth Observing Group, VIIRS Products and Services https://www.ngdc.noaa.gov/eog/viirs/ (accessed Sep 17, 2018).

(25). Elvidge CD; Zhizhin M; Hsu FC; Baugh KE VIIRS Nightfire: Satellite Pyrometry at Night. Remote Sens. 2013, 5 (9), 4423–4449.

(26). Liu Y; Hu C; Zhan W; Sun C; Murch B; Ma L Identifying Industrial Heat Sources Using Time-Series of the VIIRS Nightfire Product with an Object-Oriented Approach. Remote Sens. Environ. 2018, 204, 347–365.

(27). Scanlon BR; Reedy RC; Nicot J-P Comparison of Water Use for Hydraulic Fracturing for Unconventional Oil and Gas versus Conventional Oil. Environ. Sci. Technol. 2014, 48 (20), 12386–12393. [PubMed: 25233450]

(28). Railroad Commission of Texas: Eagle Ford Shale Oil Production 2008 through May 2018 http://www.rrc.state.tx.us/media/41519/eaglefordproduction_oil_perday.pdf (accessed Sep 18, 2018).

(29). Railroad Commission of Texas: Eagle Ford Shale Total Natural Gas Production 2008 through May 2018 http://www.rrc.state.tx.us/media/41508/eagleford_totalnaturalgas_perday.pdf (accessed Sep 18, 2018).

(30). DrillingInfo, Inc. https://info.drillinginfo.com/ (accessed Sep 17, 2018).

(31). Railroad Commission of Texas http://www.rrc.state.tx.us/about-us/resource-center/faqs/oil-gas-faqs/faq-flaring-regulation/ (accessed Aug 21, 2018).

(32). Ester M; Xu X; Kriegel H; Sander J Density-Based Algorithm for Discovering Clusters in Large Spatial Databases with Noise. Proc. 2nd Int. Conf. Knowl. Discov. Data Min. 1996, pages (AAAI Press), 226–231.

(33). McInnes L; Healy J Accelerated Hierarchical Density Based Clustering. IEEE Int. Conf. Data Min. Work. 2017, 33–42.

(34). Rinaldo A; Wasserman L Generalized Density Clustering. Ann. Stat. 2010, 38 (5), 2678–2722.

(35). Stuetzle W Estimating the Cluster Tree of a Density by Analyzing the Minimal Spanning Tree of a Sample. J. Classif. 2003, 20, 25–47.

(36). Stuetzle W; Nugent R A Generalized Single Linkage Method for Estimating the Cluster Tree of a Density. J. Comput. Graph. Stat. 2010, 19 (2), 397–418.

(37). Chaudhuri K; Dasgupta S Rates of Convergence for the Cluster Tree. Adv. Neural Inf. Process. Syst. 23 2010, 343–351.

(38). Campello R; Moulavi D; Sander J Density-Based Clustering Based on Hierarchical Density Estimates. In Advances in Knowledge Discovery and Data Mining; Pei J, Tseng VS, Cao L, Motoda H, Xu G, Eds.; Springer-Verlag, 2013; pp 160–172.

(39). Campello R; Moulavi D; Zimek A; Sander J Hierarchical Density Estimates for Data Clustering, Visualization, and Outlier Detection and Outlier Detection. ACM Trans. Knowl. Discov. Data 2015, 10 (1), 1–51.

(40). Hartigan JA Consistency of Single Linkage for High-Density Clusters. J. Am. Stat. Assoc. 1981, 76 (374), 388–394.

(41). Tedesco J; Hiller J Flares in Eagle Ford Shale Wasting Natural Gas. San Antonio Express-News. 2013.

(42). EIA. U.S. Energy Information Administration. Drilling Productivity Report: Eagle Ford Region https://www.eia.gov/petroleum/drilling/pdf/eagleford.pdf (accessed Sep 17, 2018).

(43). Polivka TN; Wang J; Ellison LT; Hyer EJ; Ichoku CM Improving Nocturnal Fire Detection with the VIIRS Day-Night Band. IEEE Trans. Geosci. Remote Sens. 2016, 54 (9), 5503–5519.

(44). Polivka TN; Hyer EJ; Wang J; Peterson DA First Global Analysis of Saturation Artifacts in the VIIRS Infrared Channels and the Effects of Sample Aggregation. IEEE Geosci. Remote Sens. Lett. 2015, 12 (6), 1262–1266.

(45). Caseiro A; Rücker G; Tiemann J; Leimbach D; Lorenz E; Frauenberger O; Kaiser JW Persistent Hot Spot Detection and Characterisation Using SLSTR. Remote Sens. 2018, 10 (7), 1–28.

(46). Carbon Dioxide Information Analysis Center (CDIAC): Global CO2 Emissions from Fossil-Fuel Burning, Cement Manufacture, and gas Flaring: 1751–2008 https://cdiac.ess-dive.lbl.gov/ftp/ndp030/global.1751_2014.ems (accessed Jan 6, 2019).

(47). Howarth RW; Santoro R; Ingraffea A Methane and the Greenhouse-Gas Footprint of Natural Gas from Shale Formations. Clim. Change 2011, 106 (4), 679–690.

(48). Field RA; Soltis J; Murphy S Air Quality Concerns of Unconventional Oil and Natural Gas Production. Env. Sci Process Impacts 2014, 16 (5), 954–969. [PubMed: 24699994]

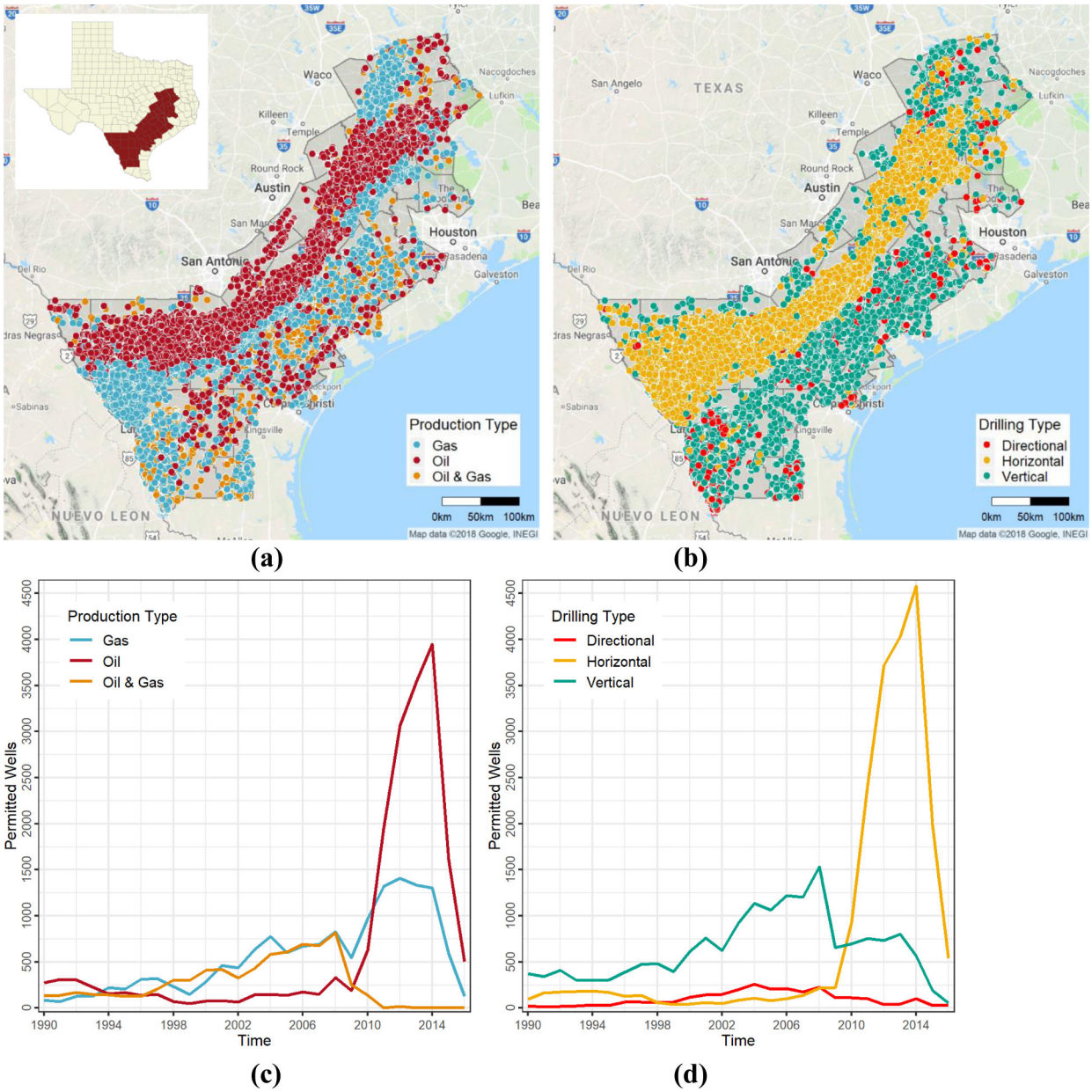

Figure 1.

The Texas Eagle Ford Shale study region, showing permitted well locations obtained from DrillingInfo by (a) production type; (b) drilling type; and the number of active wells permitted by year by (c) production type; (d) drilling type from 1990–2016. Wells that were not active during the study period between 2012–2016 are excluded.

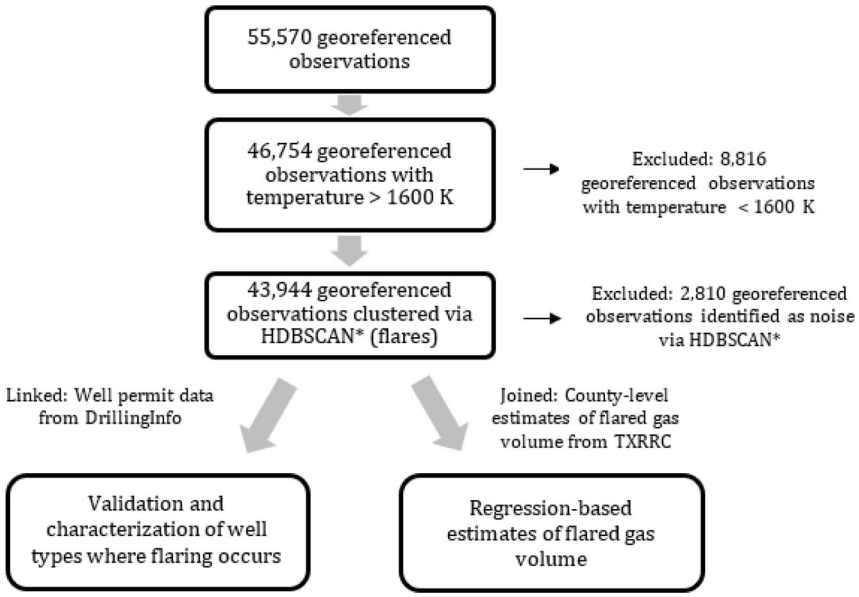

Figure 2.

Flow diagram of VIIRS Nightfire data processing for identifying flaring from oil and gas wells and estimating flared gas volume (2012–2016).

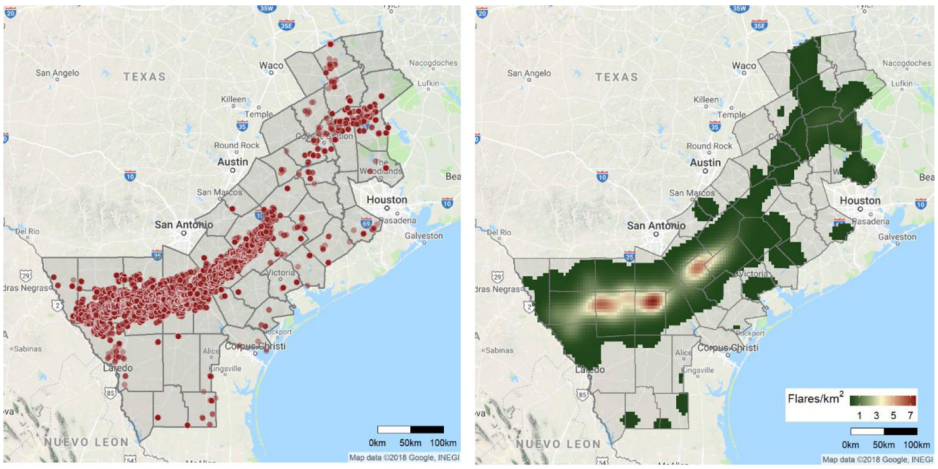

(a) **(b)**

Figure 3.

Flares identified using VIIRS Nightfire observations over the 2012–2016 study period: (a) individual flare locations N=46,754; (b) density of flares per square kilometer. Observations with temperatures < 1600K and noise points identified using HDBSCAN* are excluded.

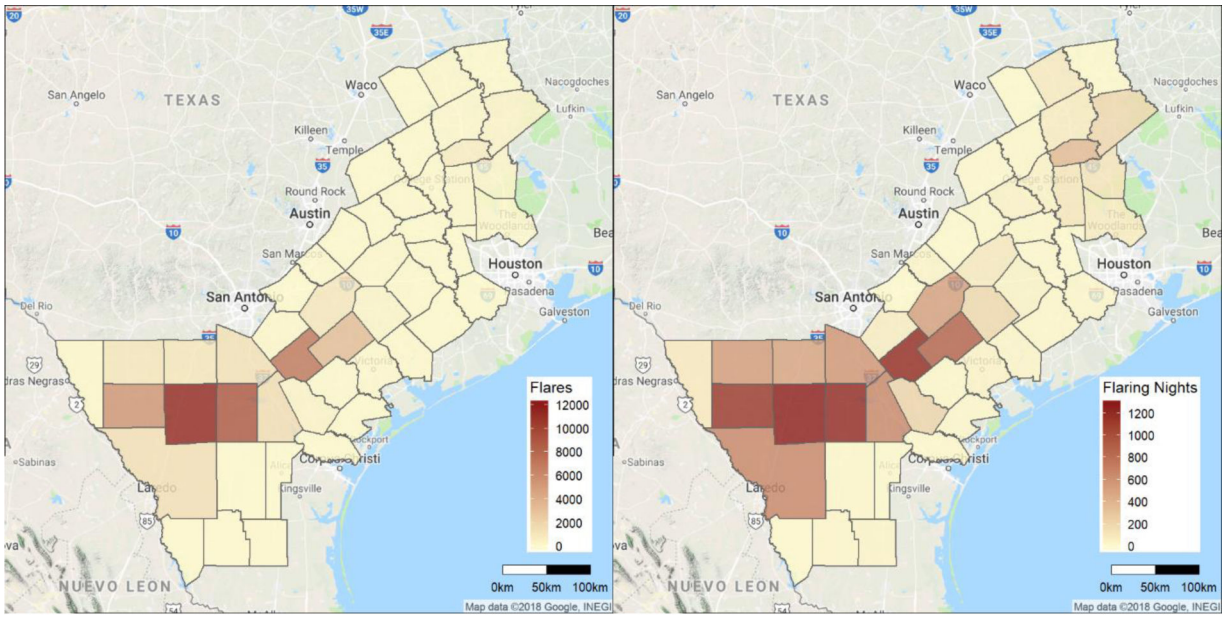

(a) (b)

Figure 4.

County representations of the total number of flares (a) and the number of nights with at least one flare in the county (b) over the 2012 to 2016 study period.

Table 1.

Production and drilling types of active permitted wells in the Texas Eagle Ford Shale during the 2012–2016 study period (total N = 41,457).

	Drill Type		
Well Production Type	**Directional**	**Horizontal**	**Vertical**
Gas	2,326	6,833	5,810
Oil	316	13,809	5,092
Oil & Gas	25	16	7,230

Table 2.

Annual summary statistics for hierarchical clustering of the nightly VIIRS Nightfire observations

Year	HDBSCAN* minPts, k	Clustered Observations (Flares), N	Noise Observations (Excluded), N (%)	Clusters, N	Ratio Flares/ Cluster
2012	5	7,773	580 (6.9%)	419	19
2013	5	9,156	679 (6.9%)	416	22
2014	6	11,816	832 (6.6%)	396	30
2015	4	10,169	437 (4.1%)	418	24
2016	3	5,030	282 (5.3%)	393	13

Table 3.

Nearest well type to flares in Eagle Ford Shale 2012–2016 (total N=43,944 flares).

	Drill Type		
Well Production Type	**Directional**	**Horizontal**	**Vertical**
Gas	63	6,382	849
Oil	178	34,057	1,616
Oil & Gas	4	2	793

Table 4.

Annual summary statistics of VIIRS flare properties and derived gas volumes.

Year	Flares N	Temperature (K) Mean (s.d)	Radiant Heat Intensity (W/m^2) Mean (s.d)	Source Area (m^2) Mean (s.d)	Per Flare Volume (BCM) Mean (s.d)	Total Flare Volume (BCM) Sum
2012	7,773	1838 (153.4)	1.51 (1.95)	2.69 (4.26)	0.029 (0.022)	0.81
2013	9,156	1842 (157.7)	1.55 (1.70)	2.65 (3.81)	0.029 (0.020)	0.99
2014	11,816	1843 (154.0)	1.68 (1.53)	2.78 (2.90)	0.031 (0.017)	1.19
2015	10,169	1851 (151.4)	1.75 (1.72)	2.86 (3.16)	0.032 (0.020)	0.99
2016	5,030	1858 (152.5)	1.74 (1.92)	2.87 (4.15)	0.032 (0.022)	0.52